

To appear in *The Astrophysical Journal*

Energy Dissipation in Multi-Phase Infalling Clouds in Galaxy Halos

Stephen D. Murray

Lawrence Livermore National Laboratory, L-22, P.O. Box 808, Livermore, CA, 94550
Electronic mail: sdmurray@llnl.gov

and

Douglas N. C. Lin

Department of Astronomy & Astrophysics, University of California, Santa Cruz CA 95064

ABSTRACT

During the epoch of large galaxy formation, thermal instability leads to the formation of a population of cool fragments which are embedded within a background of tenuous hot gas. The hot gas attains a quasi-hydrostatic equilibrium. Although the cool clouds are pressure confined by the hot gas, they fall into the galactic potential, and their motion is subject to drag from the hot gas. The release of gravitational energy due to the infall of the cool clouds is first converted into their kinetic energy, and is subsequently dissipated as heat. The cool clouds therefore represent a potentially significant energy source for the background hot gas, depending upon the ratio of thermal energy deposited within the clouds versus the hot gas. In this paper, we show that most of dissipated energy is deposited in the tenuous hot halo gas, providing a source of internal energy to replenish losses in the hot gas through bremsstrahlung emission and conduction into the cool clouds. The heating from the motion of the cool clouds allows the multi-phase structure of the interstellar medium to be maintained.

1. Introduction

The stellar velocity dispersion in the halos of galaxies similar to the Milky Way exceeds 100 km s^{-1} . The gravitational potential that binds the stars to their host galaxies is dominated by collisionless dark matter. According to the widely adopted cold dark matter

(CDM) scenario, these normal galaxies are formed through the mergers of much smaller entities, dwarf galaxies. After violent relaxation, the dark matter is well mixed in phase space and attains an extended 3-D spatial distribution. In spiral galaxies, the formation and concentration of stars in extended, flattened, rotating disks requires the detachment of ordinary matter from the dark-matter halos of the original host dwarf galaxies. The dominance of the dark-matter halo to the galactic potential at large radii, and the separation of the ordinary matter imply that, during the epoch of galactic buildup, the ordinary matter was primarily in the form of gas which dissipated a substantial fraction of its initial potential energy.

In a previous paper (Lin & Murray 2000), we considered the dynamical evolution of infalling gas in the halos of normal galaxies. We showed that for typical values ($\sim 10^6$ K) of the virial temperature, the cooling timescale increases with temperature, and the protogalactic clouds (hereafter PGC's) are thermally unstable (Field 1965). Thermal instability leads to the rapid growth of perturbations and fragmentation of a PGC (Murray & Lin 1990). The result is that a two-phase medium develops during the initial cooling of the PGC, in which a population of warm fragmentary clouds (WFC's) are confined by the pressure of hot, residual halo gas (RHG) (Burkert & Lin 2001). The RHG is cooled by radiative emission and conductive transport into the WFC's (which are efficient radiators). In our earlier work, we assumed that the RHG is heated primarily by the release of the gravitational energy as the WFC's into the central region of the halo potential, due both to their collective gravity as well as that of the dark matter. The WFC's are unable to cool below 10^4 K until their density reaches a sufficiently high value that the WFC's become self-shielded from external photo-dissociating UV radiation (Couchman & Rees 1986; Haiman, Rees, & Loeb 1997; Dong, Lin, & Murray 2003).

In the above picture, the evolution of the WFC's is similar to that of Lyman- α clouds and high velocity clouds (HVC's). Both of those systems have been proposed as representatives of late-time accretion of material in an ongoing process of galaxy buildup by mergers (Murakami & Ikeuchi 1994b; Blitz et al. 1999; Manning 1999). Because they evolve at an earlier time and closer to the centers of the parent galaxies, however, the WFC's would evolve in an environment of higher pressures and UV fluxes, compared to either Lyman- α clouds or HVC's. Their environment may, instead, more closely resemble that of cooling flows (e.g. Sarazin 1986; Loewenstein & Mathews 1987; Sarazin & White 1987, 1988), and many of our results may have relevance to those systems. Additionally, the Ly- α clouds have been proposed as being contained within dark matter “minihaloes,” (e.g. Rees 1986; Ikeuchi 1986; Mo, Miralda-Escude, & Rees 1993) whereas the WFC's are either pressure confined, or at most weakly self-gravitating

In this paper, we verify our basic conjecture that most of the gravitational energy

released by the infalling WFC’s is dissipated within the RHG. That process is crucial to the assumption that the RHG is in quasi-thermal equilibrium. Without this heating source, the background gas would gradually be depleted due to loss of thermal energy and precipitation into WFC’s. A reduction in the pressure of the background gas would also enable the WFC’s to expand and eventually eliminate the multi-phase structure of the gas. In order to simulate this process in detailed, we adopt a 2-D numerical hydrodynamic scheme with a multi-phase medium.

The motion of clouds relative to, and their interaction with an external medium has been studied by numerous authors. Murakami & Ikeuchi (1994a) examined ram-pressure stripping due to the supersonic motion of gas past clouds confined within minihalos, a very different situation from that described above for the evolution of the WFC’s. Tenorio-Tagle et al. (1986, 1987) examined the interactions of clouds hitting relatively high density galactic disks at high speeds. Again, that is a very different situation from the evolution of the WFC’s, which move slowly through a low density medium with a smooth density distribution. Murray, White, Blondin, & Lin (1993) examined the loss of gas from a cloud due to the growth of Kelvin-Helmholtz instability for transsonic motions. As with the above studies, however, the energy transfer between the cloud and the background gas was not examined.

We proceed by briefly describing our method and the model parameters in §2. In §3, we analyze the results of our computations. Finally we discuss the implication of these results in §4.

2. Numerical Method and Model Parameters

2.1. Equation of Motion

Following its collapse into the potential of the galactic dark matter halo, the RHG is shock-heated to the virial temperature of the potential, and rapidly attains a quasi hydrostatic equilibrium. For computational simplicity, we adopt a Cartesian coordinate system in which the galactic potential g is imposed in the y direction. For a spherically symmetric potential, y corresponds to the radial direction. The equation of motion of the RHG becomes

$$\frac{dV_{hx}}{dx} = -\frac{1}{\rho_h} \frac{dP_t}{dx} \quad (1)$$

$$\frac{dV_{hy}}{dy} = -\frac{1}{\rho_h} \frac{dP_t}{dy} - g \quad (2)$$

where ρ_h , P_h , $V_{h,x}$, and $V_{h,y}$ are respectively the density, pressure, two-velocity components of the RHG, $P_t = P_h + P_w$ is the total pressure, ρ_w , P_w , $V_{w,x}$, and $V_{w,y}$ are respectively the density, pressure and two velocity components of WFC's. The equation of motion for the WFC's is similar,

$$\frac{dV_{wx}}{dx} = -\frac{1}{\rho_w} \frac{dP_t}{dx} \quad (3)$$

$$\frac{dV_{wy}}{dy} = -\frac{1}{\rho_w} \frac{dP_t}{dy} - g + F_D, \quad (4)$$

where F_D is a drag force term, which is a function of the speed and geometry of the WFC's, and of their density contrast with the RHG.

2.2. Parameters for the Residual Halo Gas

We consider four models. The parameters are listed in Table 1, which lists, for each model, value of g , the polytropic index for the cloud, γ_w , the density contrast between the cloud and the background, D_ρ , and the initial downward speed of the cloud, normalized to the sound speed of the background. In all cases, the RHG is initialized with the same temperature throughout, but thereafter evolves with a polytropic equation of state, in which $P_h = K_h \rho_h^{\gamma_h}$ where K_h is the adiabatic constant, and the polytropic index $\gamma_h = 5/3$ for each model. We also assume that the RHG is initially in hydrostatic equilibrium, such that

$$\rho_h = \rho_0 e^{\frac{g}{C_h^2}(y-y_0)}, \quad (5)$$

where ρ_0 is the density at a reference height y_0 , and C_h is the isothermal sound speed of the RHG. Because the RHG initially has the same temperature throughout, the magnitude of K_h is a function of y , such that

$$K_h = C_h^2 \rho(y)^{1-\gamma_h}. \quad (6)$$

The density scale height of the RHG is

$$r_h = \frac{C_h^2}{g}. \quad (7)$$

In all models the velocities are normalized to $C_h = 1$. The initial location of the WFC's is set to be at $x_0 = y_0 = 0$. The value of g is uniform throughout the grid, justified by the fact that the computational domain represents a small fraction of a galaxy. For Models 1-3, we set $g = 0.1$, so that $r_h = 10$, while in Model 4, $g = 0.05$, giving $r_h = 20$. We set $\rho_0 = 1$. In these units, Equation (5) reduces to

$$\rho_h = e^{-g(y-y_0)}. \quad (8)$$

The computational domain extends from -0.75 to 0.75 in x , and from -15 to 1 in y . At the base of the computational domain, $\rho_h/\rho_0 \sim 4.5$ for Models 1-3, and 2.1 for Model 4.

2.3. Parameters for the Warm Fragmentary Clouds

The density ratio at the launch point, $D_\rho \equiv \rho_w/\rho_h = 10^2$ in Models 1-3, while $D_\rho = 25$ in Model 4. The magnitude of D_ρ would be constant throughout the simulation time if 1) the WFC's retain their integrity, 2) $\gamma_h = \gamma_w$, and 3) there is no shock dissipation to modify K_h and K_w . In general, however, D_ρ is a function of y , depending on the equation of state for both the WFC's and RHG.

The value $D_\rho = 100$ is selected to represent ionized clouds at temperatures of 10^4 K in a Milky Way-sized galaxy, for which the RHG is heated to the virial temperature of $\approx 10^6$ K. The smaller value of D_ρ for Model 4 would be appropriate for either cooler backgrounds or warmer clouds.

The physical dimensions of the WFC's are set by dynamical and thermal processes (Lin & Murray 2000). Clouds below a minimum radius, S_{min} , are re-heated by conduction from the RHG. The maximum radius, S_{max} , is set by the point at which the clouds become self-gravitating. Such clouds have negative specific heats, and so are unstable to external heating. The lower limit upon the cloud size translates to (Lin & Murray 2000)

$$S_{min,s} = 1.6 T_6^{3/2} D_{100}^{-1} n_{10}^{-1} \Lambda_{25}^{-1} \text{ pc}, \quad (9)$$

in the limit of saturated conduction, where T_6 is the temperature of the RHG in units of 10^6 K, D_{100} is the density contrast between the cloud and RHG in units of 100, n_{10} is number density of the cloud in units of 10 cm^{-3} , and Λ_{25} is the cooling efficiency in units of $10^{-25} \text{ ergs cm}^3 \text{ s}^{-1}$, characteristic of low metallicity gas near 10^4 K (Dalgarno & McCray 1972). In the limit of unsaturated conduction,

$$S_{min,u} = 4 T_6^{7/4} n_{10}^{-1} \Lambda_{25}^{-1/2} \text{ pc}. \quad (10)$$

The maximum cloud size is set by the Bonner-Ebert criterion for self-gravity to become important,

$$S_{max} = 350 T_4 \left(\frac{nT}{10^5} \right)^{-1/2} \text{ pc}, \quad (11)$$

where T_4 is the temperature of the WFC's in units of 10^4 K, and nT is the pressure of the clouds (assumed to be in pressure equilibrium with the RHG).

In the two-phase model discussed by Lin & Murray (2000), the WFC’s are heated by UV emission from massive stars, in a self-regulated star formation process. For the parameters given above, the total column densities of the clouds range from 5×10^{19} to 10^{22} cm $^{-2}$.

In Models 1-2 and 4, we adopt a polytropic equation of state for the WFC’s with a power index $\gamma_w = \gamma_h$. In Model 3 we attempt to maintain $\gamma_w \approx 1$ throughout the evolution. This is done by allowing the cloud to cool, but turning cooling off below a set minimum temperature, which we select as 10^4 K. The high cooling efficiency in this temperature regime ensures that the cloud temperature cannot significantly exceed the cutoff temperature. Cooling is not allowed to proceed in the background gas.

Because we are using a single-fluid code (see below), zones where cloud and background gas mix are a concern. In order to prevent significant cooling of the background gas, cooling is turned off whenever the background gas exceeds a volume fraction of 0.5, as measured by the relative amounts of the two tracers initially placed within the cloud and background. Cooling is also not allowed whenever the temperature of a cell exceeds 0.2 times the initial temperature of the background gas.

The models with polytropic equations of state permit the use of dimensionless numbers, as used here, to scale the results to a wide range of systems. The presence of cooling in Model 3, however, introduces some dimensions into the problem. In that model, we take $T_h = 10^6$ K, and $T_w = 10^4$ K, appropriate, as discussed above, for an L $_{\ast}$ galaxy. The corresponding sound speeds are $C_h = 130$ km s $^{-1}$, and $C_w = 13$ km s $^{-1}$ (assuming ionized gas). The initial density of the cloud, $n_w = 6$ cm $^{-3}$. A length dimension is not explicitly imposed upon the problem, because the heating and cooling are strictly local processes. Typical values can, however, be computed. For an isothermal potential, $g = V_c^2/R$, where V_c is the circular speed and R is the galactocentric radius. Taking $V_c = 220$ km s $^{-1}$, the physical scale height of the gas

$$R_h = \frac{C_h^2}{g} = \frac{130}{220} R = 350 R_{kpc} \text{ pc}, \quad (12)$$

where R_{kpc} is the galactocentric radius in kpc. In code units, $R_h = 10$ (see previous section), and so one unit of distance in the code corresponds to $l_{unit} = 35 R_{kpc}$ pc in physical units. The cloud radius is initially set to be 0.2 in code units, or $7 R_{kpc}$ pc in physical dimensions. The unit of time for Model 3 is given by the ratio $l_{unit}/C_h = 0.26 R_{kpc}$ Myr.

In Models 1, 3, and 4, we assume that the WFC is initially at rest. The evolution of the WFC’s is, however, dynamic, with clouds continually colliding and merging, being disrupted by dynamical instabilities, being reheated by conduction from the RHG, cooling to form stars, and condensing out of the RHG. When the clouds form from the RHG, they would be

expected to have typical speeds up to the sound speed of the RHG. In Model 2, therefore, we take the WFC to be initially falling in the $-y$ direction, at a velocity equal to C_h .

Due to their negative buoyancy, the WFC’s fall through the RHG in all models. If the background RHG is not perturbed, it induces a drag force F_D on WFC’s. For WFC’s with sizes S which are larger than the mean free path of particles in the RHG,

$$F_D = \frac{1}{2} C_D \pi S^2 \rho_h V_w^2, \quad (13)$$

where C_D is the drag coefficient, and S is the cloud radius (Batchelor 2000). In flows with high Reynolds number, the turbulent wake behind the body provides an effective momentum transfer mechanism, dominating C_D . For example, the experimentally measured C_D for a hard sphere in a nearly inviscid fluid is 0.165 (Whipple 1972). For compressible gas clouds, C_D is probably closer to unity.

When $F_D \approx g$, the WFC’s attain a terminal speed

$$V_t \approx \left(\frac{8D_\rho S g}{3C_D} \right)^{1/2}. \quad (14)$$

At the launch point, the size of the WFC is set to be $S(y_0) = 0.2$ in models 1-3. If $C_D = 1$ and the WFC preserves its integrity, $V_t = 2.3$, which would exceed sound speed of the RHG. Once the Mach number of the WFC exceeds unity, however, shock dissipation would greatly increase the drag relative to the above estimate. Prior to the WFC achieving $V \approx 1$, however, Rayleigh Taylor instability causes it to break up into smaller pieces. For smaller fragments, the value of V_t is reduced, as seen in Equation (14). Due to shock dissipation, the sound speed in the RHG is also slightly larger than that in Equation (14). Both of the above factors may prevent the falling WFC’s from attaining $V_t > C_h$. Because the WFC’s are pressure confined, however, their internal sound speed $C_w = D_\rho^{-1/2} C_h = 0.1 \ll V_t$, and so internal shock dissipation is likely to occur within the WFC’s. In order to examine the role of the relative magnitudes of the speeds, we choose, in model 4, $S(y_0) = 0.1$, $g = 0.05$, and $D_\rho(y_0) = 25$ such that $V_t < C_h$ throughout the computational domain. Shock dissipation does not occur in the RHG, but it is present interior to the WFC.

In Model 3, we assume the same initial condition as model 1, but adopt an effectively isothermal equation of state for the WFC’s by allowing the gas to cool to 10^4 K. The resulting energy drainage would lead to a greater dissipation rate within the WFC’s but it should not significantly modify the energy deposition rate into the RHG.

2.4. Numerical Method

The models discussed below are calculated using *Cosmos*, a multi-dimensional, chemo-radiation-hydrodynamics code developed at Lawrence Livermore National Laboratory (Anninos, Fragile & Murray 2003). For the current models, radiative emission is not included. In order to maximize the resolution, the models are run in two dimensions. Because *Cosmos* runs on a Cartesian grid, this means that the clouds simulated are actually slices through infinite cylinders, rather than spheres. This limitation should not, however, significantly alter our conclusions, and allows us to run the simulations at significantly higher resolution than would be possible in three dimensions. The resolutions of the models are 300x3200 zones. The clouds are therefore resolved by 80 zones across their diameters. This is somewhat poorer than the resolution found necessary by Klein, McKee, & Colella (1994) for their study of shock-cloud interactions. Because the clouds in our models are not subject to extreme shocks, however, lower resolutions should be adequate, and reductions in resolution by a factor of two have not been found to have any affect upon our results.

Because we are concerned with energy transfer and dissipation, the form of the artificial viscosity used in the models might be expected to play a significant role. In order to examine that possibility, we have computed versions of Model 1 using both scalar and tensor forms of the artificial viscosity, with the coefficient varied by a factor of two, and both with and without linear artificial viscosity. The energy changes in the cloud and background were found to differ among the models by no more than 10%. We therefore conclude that the form of the artificial viscosity does not dominate our results. The lack of sensitivity is most likely to the absence of strong shocks in the models.

The models are run with reflecting boundary conditions on all sides. This choice of boundaries serves to isolate the system, eliminating potential ambiguities in the interpretation of the energies of the two components.

3. Results of the Numerical Simulations

3.1. Model 1: Transsonic sedimentation of adiabatic clouds

In Model 1, we adopt a polytropic equation of state for both the cloud and background. For the values of D_ρ , S , and g of the model, $V_t \sim C_h$ during the descent.

In Figure 1, we show the evolution of the density of Model 1. The model is shown from time 0 to 16, at intervals of 2 (the horizontal sound crossing time in the RHG $\Delta x/C_h = 1.5$). The WFC rapidly accelerates to a speed $|V_y| \approx C_h$, at which point the increasing drag causes

it to achieve a terminal speed. The deceleration of the cloud as it approaches terminal speed leads to the growth of Rayleigh-Taylor instability, causing rapid breakup of the cloud. For an incompressible fluid, the Rayleigh-Taylor instability grows, in the linear regime, as $e^{\omega t}$, where

$$\omega^2 = \frac{2\pi g}{\lambda} \left(\frac{\rho_h - \rho_l}{\rho_h + \rho_l} \right), \quad (15)$$

λ is the wavelength of the perturbation, and the subscripts h and l refer, respectively, to the heavy and light fluids (Chandrasekhar 1961, p. 428). For subsonic flows, the growth rate is similar for compressible fluids. Perturbations with the shortest wavelengths grow most rapidly, but saturate quickly when their amplitudes $A \approx \lambda$. As a result, wavelengths $\lambda \sim S$ lead most strongly to cloud breakup. For such perturbations, the above relation gives $\omega \approx 17$, in fair agreement with the rate of breakup observed in the cloud, though the latter is complicated by the additional growth of Kelvin-Helmholtz instability due to the flow of gas around the cloud (cf. Murray et al. 1993).

Figure 2 shows the energy evolution of Model 1. Shown are the evolution of the total (internal, kinetic, and gravitational), the kinetic plus internal, kinetic, and internal energies. Values for the background gas are given by the solid curves, while those for the cloud are indicated by the dashed curves. The energies are in code units, and are plotted as changes relative to their initial values. The energies of the cloud and background are calculated as sums across the entire computational grid, with the contribution from each zone weighted by the fractional amount of the appropriate tracer present in each zone. This should minimize any confusion due to mixing of the cloud and background gas. The high order of the advection scheme also minimizes numerical diffusion (Anninos, Fragile, & Murray 2003).

As can be seen in Figure 2, the total energy of the cloud decreases as it falls in the gravitational potential. The increase in E_{Tot} at late times is due to the upward motion of cloud material entrained within the vortices that form behind the cloud. The kinetic energy of the cloud increases until it reaches a terminal infall speed at $t \approx 10$. According to Equation (14), the terminal speed of infalling clouds is an increasing function of their size. As a cloud breaks up into many smaller pieces, its kinetic energy decreases along with V_t . The internal energy of the cloud does not change significantly during its descent and breakup. The distance travelled before breakup is $\sim 30S(y_0)$. The effective cross section of the cloud is $\sim 2S(y_0)$, implying that the mass of the RHG that is encountered by the falling cloud is smaller than, but comparable to the mass of the cloud (Murray et al. 1993). During break up, the terminal velocity of the fragments $V_t \propto S^{1/2}$, in accordance with Equation (14). The fragments therefore trail behind the remaining clouds.

The kinetic, and especially the internal energy of the background gas are substantially increased by the end of the simulation. In this model, therefore, the majority of the energy

released by the infall of the cloud is deposited into the internal energy of the background gas, primarily by the action of weak shock waves generated by the motion of the infalling cloud. This result supports the assumption of Lin & Murray (2000) that the rate of energy deposition throughout the galaxy is directly proportional to the total infall rate of WFC's throughout the system.

3.2. Model 2: Supersonic impact of WFC's

In Model 1, the WFC attains a terminal speed which is a significant fraction of both C_h , and the value of V_t predicted from Equation 14. It might also be expected that WFC's which condense from the RHG would have initial speeds comparable to the sound speed of the RHG. In order to examine the possible effects of nonzero initial speeds upon the evolution, we consider in Model 2 an initial condition in which the WFC is already falling at the sound speed at the start of the numerical calculation.

The density of Model 2 is shown in Figure 3. Due to the more rapid motion of the cloud, as compared to that of Model 1, the simulation is only carried out to $t = 12$. The initial motion of the cloud can be seen to drive a weak shock ahead of it. Behind the shock, the leading edge of the cloud continues to move downwards at almost C_h , slowing down gradually until the very end of the simulation, when it rapidly decelerates as it breaks up, due to the combined action of Rayleigh-Taylor and Kelvin-Helmholtz instabilities. These results suggest that the infalling WFC's quickly settle to V_t irrespective of the initial conditions, as we have assumed previously (Lin & Murray 2000). The breakup of the cloud proceeds at nearly the same vertical height as in Model 1. The similarity arises because the models have the same gravitational accelerations and density contrast. Prior to breakup, the downward motion of the cloud is more rapid than the value of V_t found for Model 1. The differences are due to the modification in the drag caused by the leading shock in Model 2.

The energy evolution is shown in Figure 4. The initial kinetic energy of the cloud, $E_{K,0} = 6.3$, is almost entirely dissipated by $t = 10$. Over the same time interval, the cloud is also able to penetrate to a greater depth than the cloud in Model 1, increasing the release of gravitational energy relative to that model. Together, these effects lead to a gain of internal energy for the background gas by a approximately a factor of two larger than seen in Model 1.

However, the depth at which the cloud breaks up is similar in the two models. As in Model 1, the break up occurs when the cloud encounters a column of RHG that is comparable in mass to that of the cloud. Thereafter, the fragments' rate of sedimentation is significantly reduced in accordance with Equation (14). The asymptotic rate of RHG's internal energy

increase in Model 2 is comparable to that in Model 1.

3.3. Model 3: Efficient energy loss within the cool clouds

In Model 3, we approximate an isothermal equation of state for the cloud, as described above, in order to represent the limit in which cooling is highly efficient. The evolution of the density is shown in Figure 5, while the energies are shown in Figure 6. The isothermal behavior of the cloud leads to nonconservation of the total energy of the cloud plus background, and so we do not plot that here, focusing instead upon the kinetic and internal energies.

As expected, cooling within mixed cells does lead to some cooling of the background gas, as well as some overcooling within the cloud, both of which can be seen in Figure 6. The lack of heating within the cloud leads to additional compression relative to the previous models, reducing its breakup. Overall, however, the transfer of kinetic energy of the cloud to the internal energy of the background gas is very similar to the adiabatic models described above, indicating that efficient cooling within the clouds does not have a strong effect upon the energy deposition rate.

Fragmentation of the cloud also occurs in Model 3. The efficient cooling enhances the density contrast between the cloud and the RHG, such that the cloud retains smaller volume and cross section. Consequently, the cloud encounters a smaller gas mass along the path of its descent, and fragmentation occurs at a greater depth. On small wavelengths, the infalling cloud appears to be better preserved than in the previous models. But on the scale of the cloud size, the cloud again fragments after encountering a column similar to its own mass, as above.

3.4. Model 4: Subsonic Sedimentation of WFC’s

For Model 4, $D_\rho = 25$, and $g = 0.05$, such that V_t is predicted by Equation 14 to be subsonic. The evolution of the density of Model 4 is shown in Figure 7. The cloud rapidly reaches a terminal speed, $V_t \approx 0.3$, smaller than predicted if $C_D = 1$. As in Model 1, however, expansion of the cloud enhances the drag coefficient to $C_D > 1$. The cloud therefore never achieves the terminal speed predicted for a hard sphere, even in the absence of strong supersonic dissipation. From Equation 15, $\omega \approx 6$, and the cloud breaks up even more rapidly than the more dense clouds considered in Models 1-3, due to its reduced density contrast relative to those models.

The downward displacement of the cloud in Model 4 is reduced by a factor of a few relative to that of Model 1. As a result, the gravitational energy released by the settling of the cloud, and dissipated into the background gas, is reduced by an order of magnitude relative to Model 1, as can be seen in Figure 8.

In the absence of trans/supersonic motion of the cloud through the background, shock dissipation cannot be a strong mechanism for the dissipation of energy due to motion of the cloud. The primary mechanism involves the wake of the cloud. In the simulations, the vortical motions behind the cloud dissipate energy on small scales, due to artificial and numerical viscosity. In three dimensions, the high Reynolds numbers would lead to the formation of turbulent wakes, which would lead to the dissipation of energy by viscous stress on sufficiently small length scales, leading to the same outcome as observed in Model 4. The observed outcome of the energy deposition is not, therefore, sensitive to the exact physical process responsible for it.

4. Summary and Discussion

In this paper, we examine the interactions of a two-phase medium in a passive gravitational potential. This situation represents the physical environment that occurs naturally in the context of galaxy formation, cooling flows, and during the transition of gas clouds from quasi-hydrostatic contraction to dynamical collapse. It is a natural consequence of thermal instability, which generally leads to the emergence of a population of relatively cool, dense clouds (warm, fragmentary clouds, or WFC’s) that are pressure confined by an ambient hot, tenuous gas (residual hot gas, or RHG). In such a state, the hot gas establishes a quasistatic equilibrium with the background gravitational potential, and the cold clouds settle into it under the action of their negative buoyancy. In the present investigation, we neglect the self-gravity of the gas, and consider the potential to be due to a time-invariant background distribution of dark matter or stars.

Through a series of numerical simulations, we demonstrate the following evolutionary outcomes.

- 1) During their descent, the WFC’s break up on the same timescale as is required for them to attain a terminal speed.
- 2) Most of the energy released from the sedimentation of the WFC’s into the background gravitational potential is deposited into the RHG.

These results provide justifications for the assumptions we made in our earlier model for

the evolution of multi-phase medium during the epoch of galaxy formation (Lin & Murray 2000). They also resolve an outstanding conceptual issue with regard to the energy source needed for the persistence of the multi-phase medium. In particular, the RHG can achieve a thermal equilibrium, in which its heat loss via bremsstrahlung emission and conduction into the WFC's is balanced by the release of energy from the infalling WFC's. This equilibrium allows a multi-phase structure to be maintained in the system.

The equilibrium is very dynamic. The WFC's are continually formed by thermal instability within the hot gas. As they move within the hot gas, they break up, and are eventually re-heated by conduction from the hot gas. They may also cool and form stars, if local sources of UV radiation are lost. Additionally, the fragmentation of the WFC's increases their surface area to volume ratio. This reduces their timescale for collisions and mergers, leading to the formation of larger WFC's. A natural extension of the present investigation, therefore, is to consider the collisional equilibrium for a population of WFC's. We shall investigate this in future work.

This work was performed under the auspices of the U.S. Department of Energy by University of California, Lawrence Livermore National Laboratory under Contract W-7405-Eng-48. This work is partially supported by NASA through an astrophysical theory grant NAG5-12151.

REFERENCES

Anninos, P., Fragile, P. C. & Murray, S. D. 2003, *ApJS*, 147, 177

Batchelor, G. K. 2000, An Introduction to Fluid Dynamics, (Cambridge: Cambridge University Press), 331

Blitz, L., Spergel, D. N., Teuben, P. J., Hartmann, D., & Burton, W. B. 1999, *ApJ*, 514, 818

Burkert, A., & Lin, D. N. C. 2000, *ApJ*, 537, 270

Chandrasekhar, S. 1961, Hydrodynamic and Hydromagnetic Stability, (New York: Dover)

Couchman, H. M. P., & Rees, M. J. 1986, *MNRAS*, 221, 53

Dalgarno, A., & McCray, R. A. 1972, *ARA&A*, 10, 375

Dong, S., Lin, D. N. C., & Murray, S. D. 2003, *ApJ*, 596, 930

Field, G. B. 1965, *ApJ*, 142, 531

Haiman, Z., Rees, M. J., & Loeb, A. 1997, *ApJ*, 476, 458

Ikeuchi, S. 1986, *Ap&SS*, 118, 509

Klein, R. I., McKee, C. F., & Colella, P. 1994, *ApJ*, 420, 213

Lin, D. N. C., & Murray, S. D. 2000, *ApJ*, 540, 170

Loewenstein, M. & Mathews, W. G. 1987, *ApJ*, 319, 614

Manning, C. V. 1999, *ApJ*, 518, 226

Mo, H. J., Miralda-Escude, J., & Rees, M. J. 1993, *MNRAS*, 264, 75

Murakami, I. & Ikeuchi, S. 1994, *ApJ*, 420, 68

Murakami, I. & Ikeuchi, S. 1994, *ApJ*, 421, L79

Murray, S. D., & Lin, D. N. C. 1990, 363, 50

Murray, S. D., White, S. D. M., Blondin, J. M., & Lin, D. N. C. 1993, *ApJ*, 407, 588

Rees, M. J. 1986, *MNRAS*, 218, 25P

Sarazin, C. L. 1986, *RvMP*, 58, 1

Sarazin, C. L. & White, R. E. 1987, *ApJ*, 320, 32

Sarazin, C. L. & White, R. E. 1988, *ApJ*, 331, 102

Tenorio-Tagle, G., Bodenheimer, P., Rozyczka, M., & Franco, J. 1986, *A&A*, 170, 107

Tenorio-Tagle, G., Bodenheimer, P., Rozyczka, M., & Franco, J. 1987, *A&A*, 179, 219

Whipple, F. L. 1972, in *From Plasma to Planet*, ed. A. Elvius, (London: Wiley)

Table 1. Model Parameters

Model	g	γ_w	D_ρ	$V_{y,0}/C_h$
1	0.10	$\frac{5}{3}$	100	0
2	0.10	$\frac{5}{3}$	100	-1
3	0.10	1	100	0
4	0.05	$\frac{5}{3}$	25	0

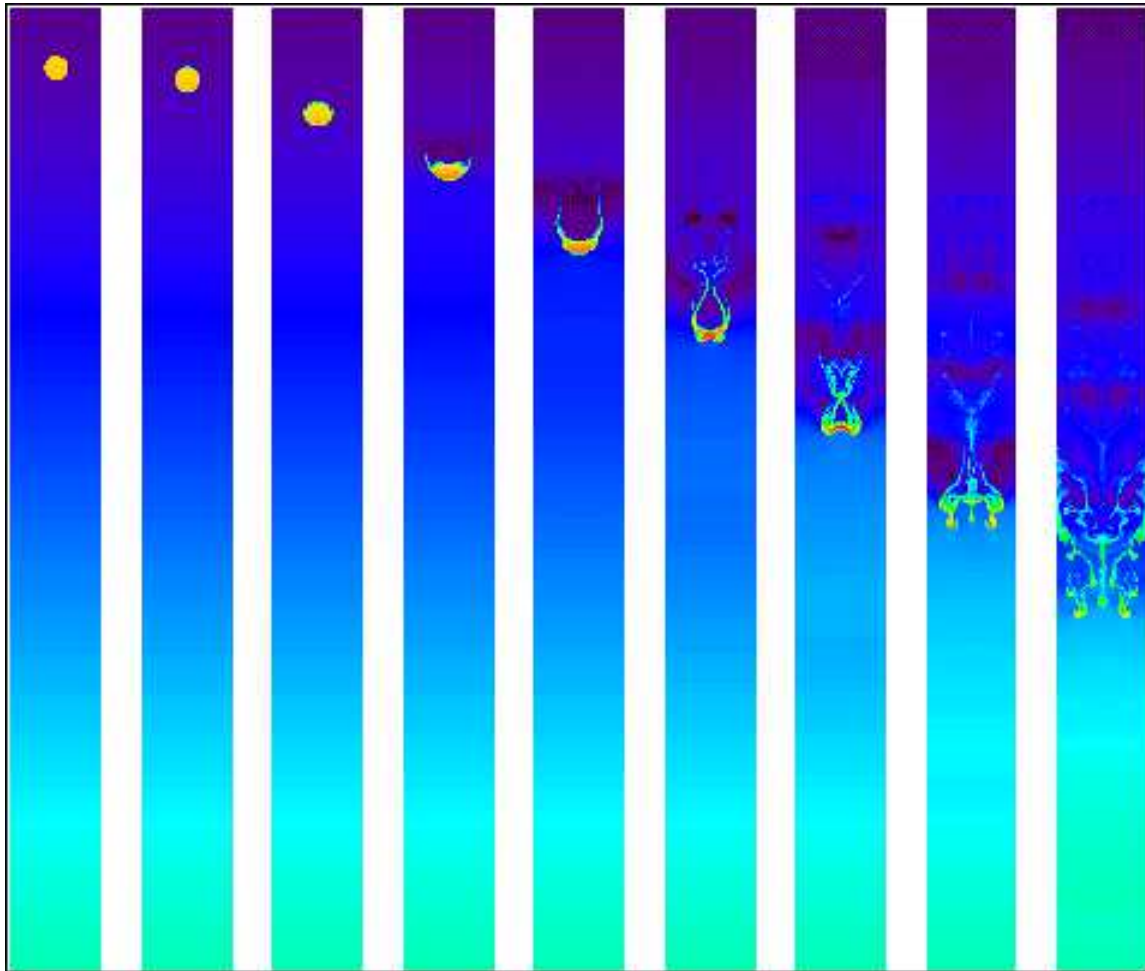


Fig. 1.— Density evolution of Model 1. The model is shown from $t = 0$ to 16, in intervals of 2, where the horizontal sound crossing time is 1.5.

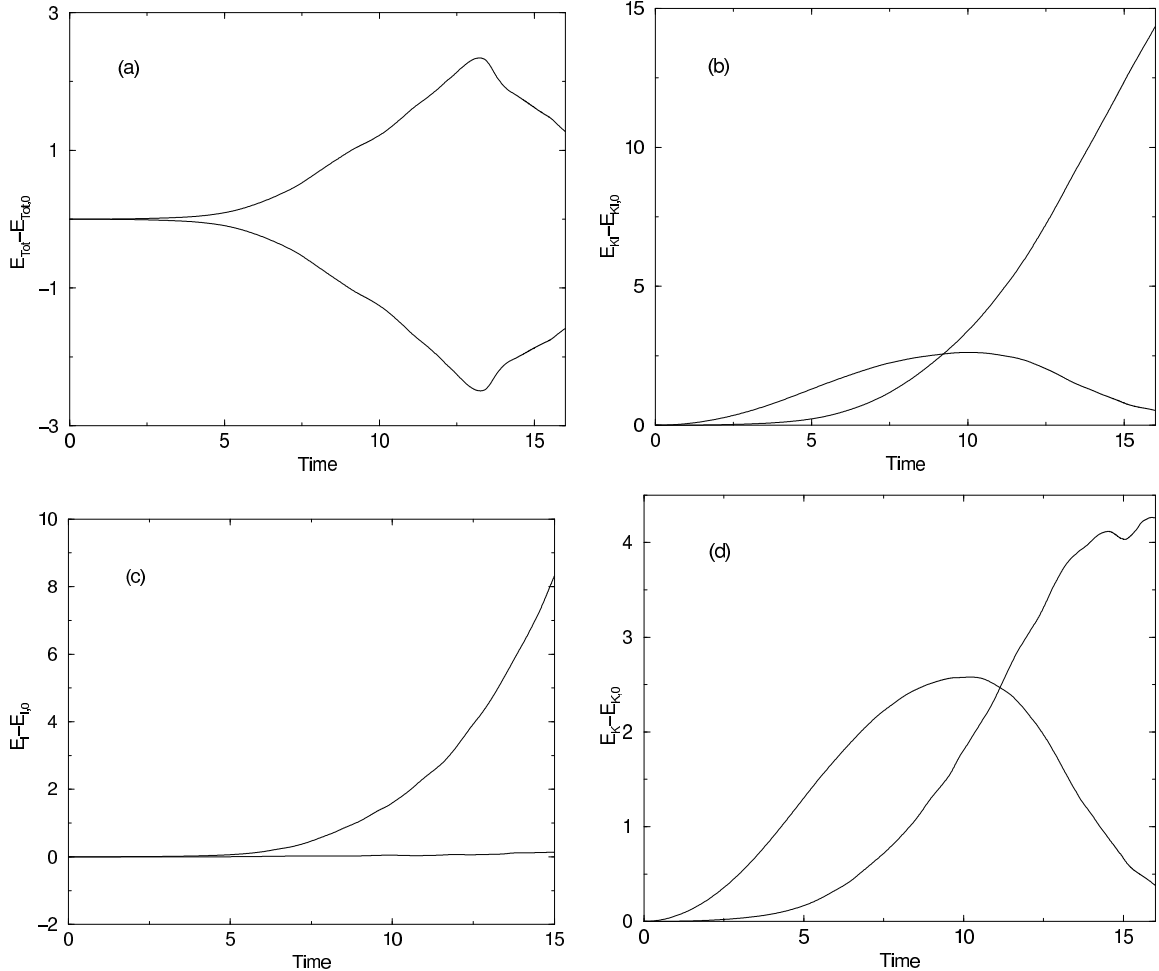


Fig. 2.— Energy evolution of Model 1. Shown are the time evolution of the (a) total, (b) kinetic plus internal, (c) internal, and (d) kinetic energies. Data for the background gas are shown as the solid curves, while that for the dense cloud are shown as dashed curves.

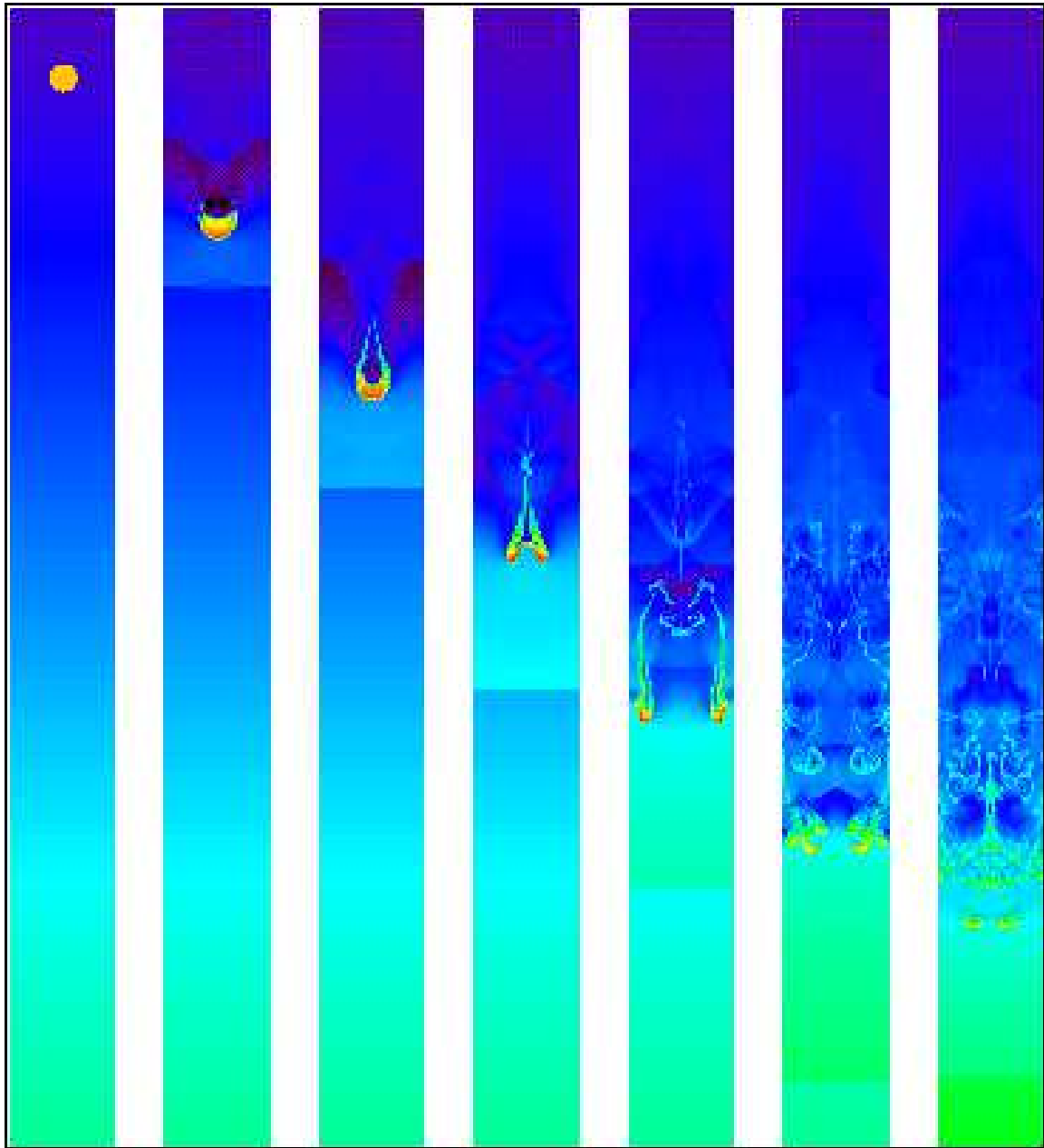


Fig. 3.— Density evolution of Model 2, displayed as in Figure 1. Due to the rapid motion of the cloud, the simulation is only carried out to $t = 12$.

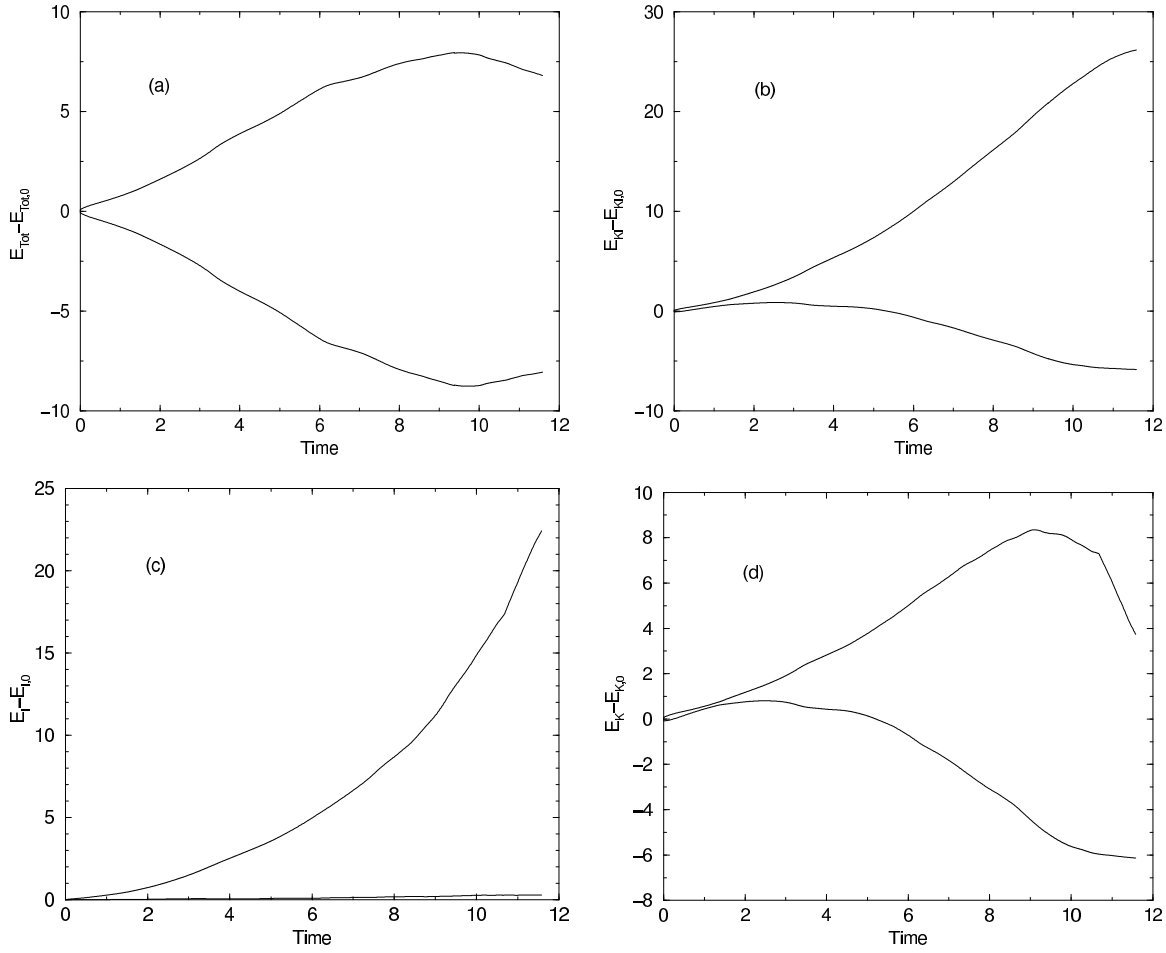


Fig. 4.— Energy evolution of Model 2, displayed as in Figure 2.

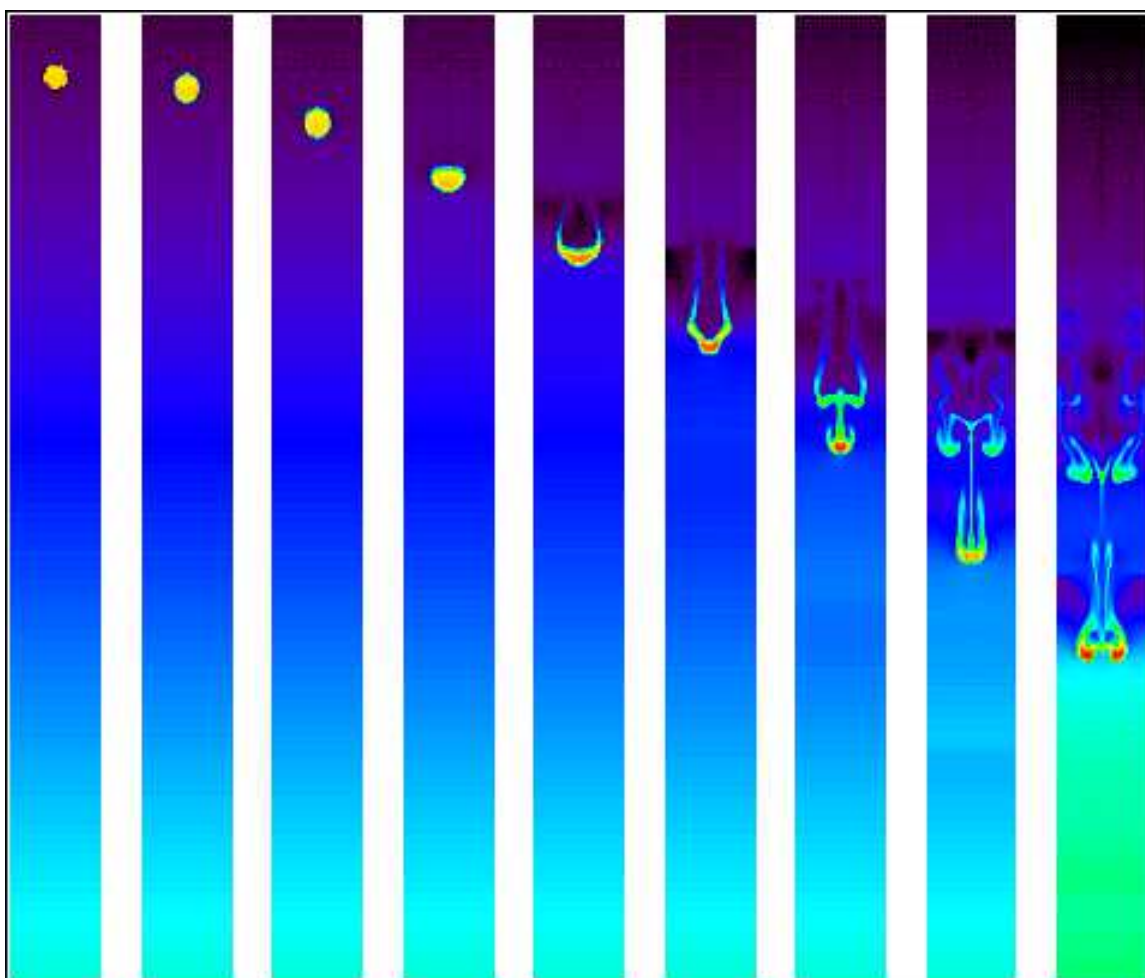


Fig. 5.— Density evolution of Model 3, displayed as in Figure 1.

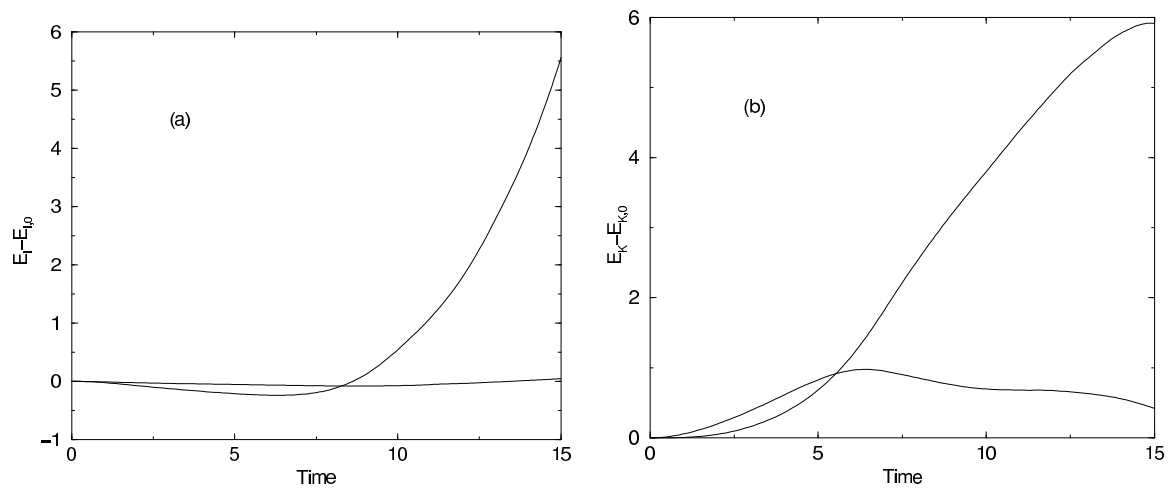


Fig. 6.— Energy evolution of Model 3, displayed as in Figure 2.

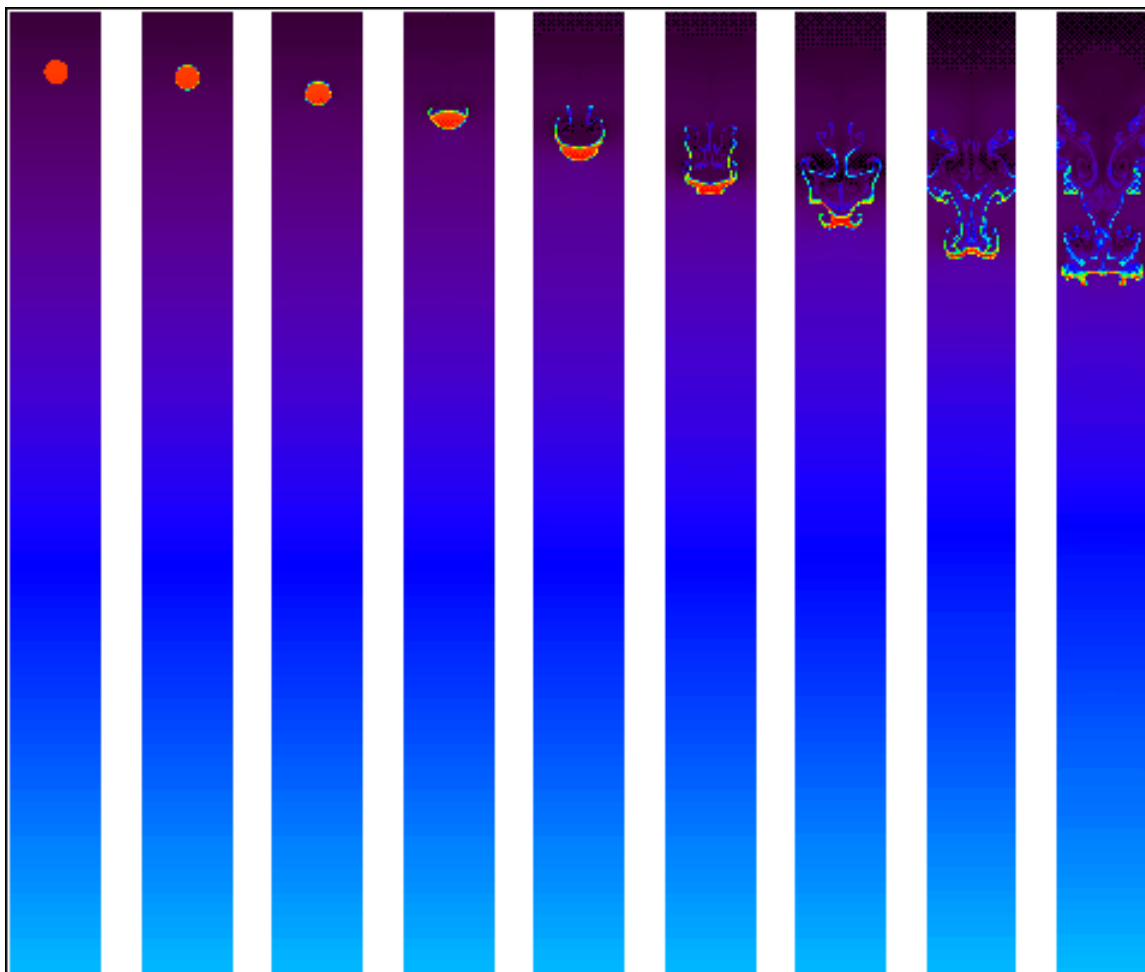


Fig. 7.— Density evolution of Model 4, displayed as in Figure 1.

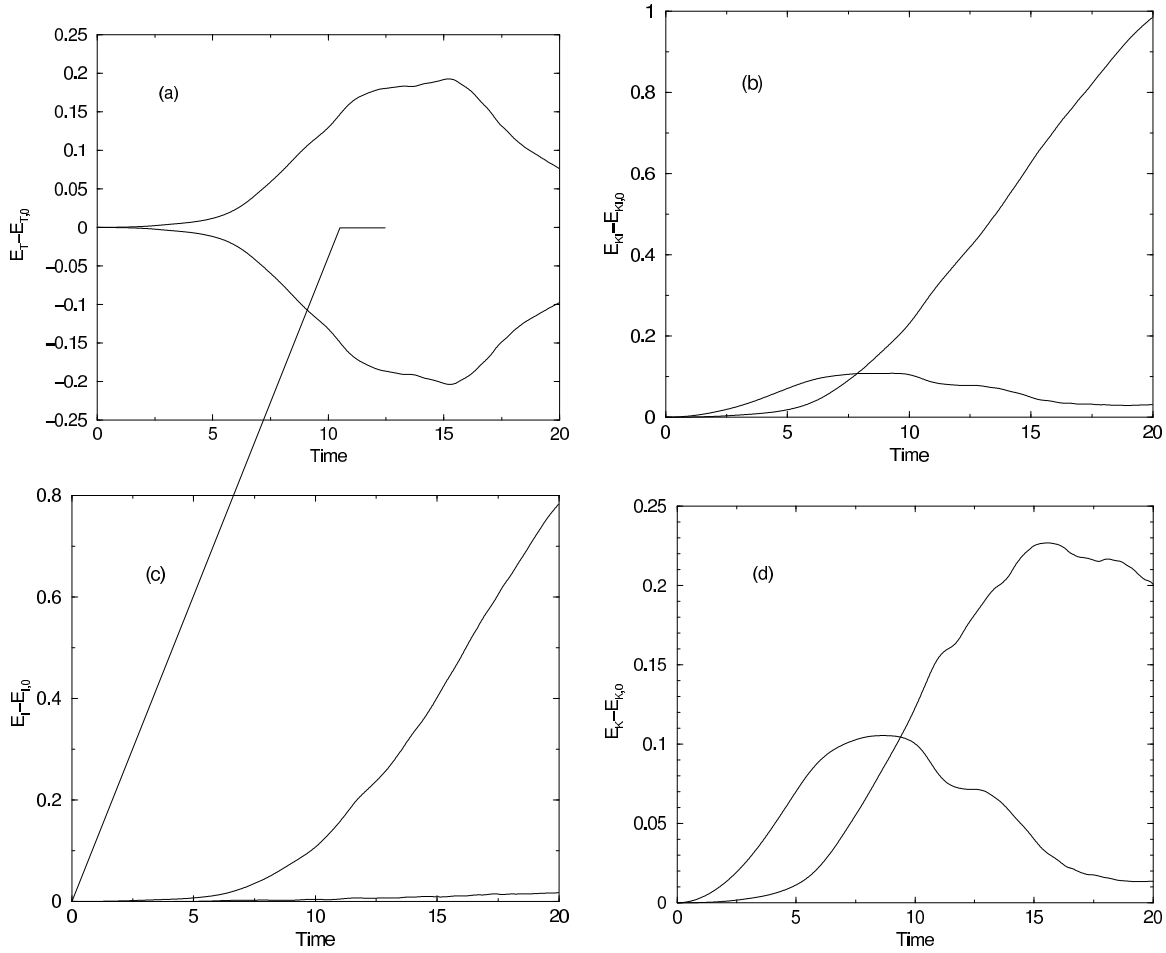


Fig. 8.— Energy evolution of Model 4, displayed as in Figure 2.

